Proceedings of the Twelfth International Conference on
Engineering Computational Technology
Edited by: P. Iványi, J. Kruis and B.H.V. Topping
Civil-Comp Conferences, Volume 8, Paper 2.2
Civil-Comp Press, Edinburgh, United Kingdom, 2024
ISSN: 2753-3239, doi: 10.4203/ccc.8.2.2

Parallel Enclosed Hole Detection for Introducing Manufacturing Constraints in Topology Optimization

D. Herrero-Pérez

Department of Structures, Construction and Graphic Expression, Technical University of Cartagena, Cartagena, Spain

Abstract

This work presents a distributed approach based on Graph Theory for detecting enclosed holes in density-based topology optimization using the traditional material penalization scheme. The distributed topology optimization framework divides the domain into several subdomains to exploit parallel computing resources. The proposal generates a set of graphs from the empty elements of the meshes of such subdomains, detecting the empty regions and classifying them. Then, it generates a hierarchical distributed graph between the subdomains to obtain a coherent representation of the connectivity design, minimizing inter-node communications in the classification of the empty regions. We use such information to introduce manufacturing constraints preventing enclosed holes in the final designs, which is especially useful in diverse additive manufacturing techniques because such holes can induce failures in the manufacturing process. We validate the proposal using a classical two-dimensional cantilever problem with asymmetric simplifications and parallel computing.

Keywords: connectivity, topology optimization, enclosed holes, high-performance computing, additive manufacturing, computational effort.

1 Introduction

Topology optimization techniques provide innovative and high-performance designs by minimizing a cost function subjected to constraint sets. Commonly, we consider these results conceptual designs because they are complex to manufacture using standard manufacturing techniques. Additive Layered Manufacturing (ALM) techniques can manufacture directly the complex geometries provided by topology optimization techniques [1] using a layer-by-layer strategy, obtaining significantly high-performance and lightweight structural parts.

In the case of minimizing compliance [2], it is usual to obtain designs with cavities and enclosed holes. Such holes and cavities contribute to compliance minimization or stiffness maximization of designs. However, they can complicate the manufacturing process depending on the additive manufacturing technique. The enclosed cavities are undesirable for many ALM technologies, such as Selective Laser Sintering (SLS), Stereolithography (SLA), and Fused Deposition Modeling (FDM) [3]. In the first two manufacturing techniques, we should remove the not sintered powders or resins that serve as support material after fabrication. This process is not feasible in enclosed cavities, which induces problems depending on the material used. Besides, we cannot remove the support structures in the latter ALM technology after the fabrication of the optimized design.

We focus on removing the enclosed cavities in topology optimization using compliance minimization. We usually formulate removing enclosed holes as a manufacturing constraint of ALM. We can find different approaches addressing this problem in the literature. A widely adopted approach is forcing the design to be a simply connected structure [4], introducing the requirement of eliminating the enclosed cavities as a connectivity constraint in the topology optimization formulation. Some works use this approach transforming the connectivity constraint into an equivalent problem, such as a temperature constraint in the Virtual Temperature Method (VTM) [5] and an electrostatic one using the Poisson method [6]. Another approach consists of imposing the void phase connectivity by constraining the algebraic connectivity in the context of Graph Theory [7]. We also find several works removing the enclosed cavities with heuristic methods using evolutionary topology optimization methods, such as pathfinding schemes [8] and hole-filling approaches [9]. Another possibility is using restriction methods to gradually smooth the holes and cavities by controlling the topology of the design. We can mention persistent homology approaches to introduce topological constraints in the optimization process [10]. In this work, we adopt a similar approach to penalize the enclosed cavities during the topology optimization process.

Another key factor to address topology optimization incorporating manufacturing constraints in real-world problems is the computational effort. High-performance computing (HPC) has shown effectiveness in increasing the computing performance using multi-core [11] and many-core [12] computing in the context of topology opti-

mization. We can also improve the computing performance using hierarchical parallelization schemes in the context of topology optimization [13, 14]. For these reasons, we develop the tools needed to take advance of the computing resources of modern computer system infrastructures both in the detection of enclosed cavities and the topology optimization introducing manufacturing constraints.

We organize the remainder of the manuscript as follows. We devote Section 2 to identifying connected empty regions and their classification. The objective to detect enclosed cavities efficiently using parallel computing. Section 3 reviews the basis and theoretical background of density-based topology optimization and the modifications needed to incorporate the manufacturing constraints preventing enclosed cavities in the resulting design. Section 4 presents the numerical experiments evaluating the performance, feasibility, and scalability of the techniques adopted for taking advantage of parallel multi-core computing in density-based topology optimization incorporating manufacturing constraints. Finally, Section 5 presents the concluding remarks of the proposal.

2 Enclosed hole detection

Adopting a density-based topology optimization approach, we relax the solid/void material distribution representation characterizing composite materials [15] by interpolating the material properties. In particular, we use the Solid Isotropic Material with Penalization (SIMP) method [2], which links the elastic modulus of elemental stiffness and the continuous design variables $\rho(x)$ as

$$E(\rho) = \rho^p E_0, \tag{1}$$

where E_0 is the elastic modulus for the solid material and $p > 1$ is the penalization power. We can use he elemental design variable of $\rho(x)$ of the topology optimization approach to decide if the elements correspond to solid or void regions by thresholding. We can then define the domain as

$$\Omega = \Omega^v \cup \Omega^s, with \begin{cases} \Omega^v : x \in \{\rho \leq \rho_{th}\} \\ \Omega^s : x \in \{\rho > \rho_{th}\} \end{cases} \tag{2}$$

where Ω^s is the solid region, Ω^v is the void region, and ρ_{th} is the thresholding value of the design variable.

We then use the connectivity concept [16] to adopt a simple strategy for detecting and classifying holes from the domain Ω^v during the design process using Graph Theory. The approach consists of the following tasks using the elements of the domain Ω^v: (i) labeling the elements in the boundary, (ii) generating disconnected graphs from elements, and (iii) labeling the graphs into open voids Ω^{ov} and enclosed voids Ω^{ev} with $\Omega^v = \Omega^{ov} \cup \Omega^{ev}$ depending on they contain elements in the boundary or

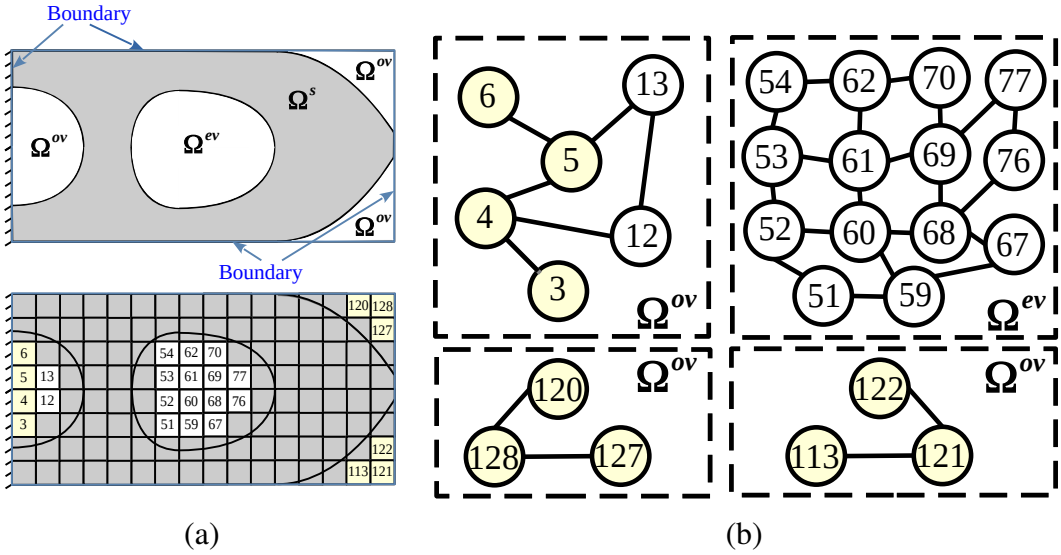

Figure 1: Detection of enclosed holes: (a) the multiply connected structure and the binarized design field labeled by boundary edges, and (b) the undirected disconnected graphs for detecting holes and classifying them into opened and enclosed ones.

not, respectively. We generate the undirected graphs from the domain Ω^v using the elements as graph nodes and the edges or faces between elements as the arcs of the undirected graph. We then use the breadth-first search method [17] to find the disconnected graphs representing the empty regions in the domain Ω^v. The breadth-first search method is the most efficient graph search approach for undirected graphs. Finally, we classify the disconnected graphs of the domain Ω^v as *opened voids* Ω^{ov} and *enclosed voids* Ω^{ev}. The former has labeled nodes in the boundary, whereas the latter does not have them.

Figure 1 shows a simple example of the hole detection and the classification of void cavities. Figure 1(a) depicts a design field binarized using the criteria of equation (2) with the threshold ρ_{th}. It also shows the yellow labeled elements depending on whether their edges or faces are in the boundary. Figure 1(b) shows the disconnected undirected graphs generated with domain Ω^v using the breadth-first search method. It also shows the classification of cavities as Ω^{ov} or Ω^{ev} depending on the nodes of disconnected graphs labeled as containing a boundary edge or face.

We parallelize the proposed approach to find enclosed cavities by partitioning the domain into n parts as $\Omega = \Omega_1 \cup \cdots \cup \Omega_n$. We then follow the same approach as in the serial counterpart to find the set of disconnected graphs classified as Ω^{ov} or Ω^{ev}. Such subdomains keep the sharing edges or faces between subdomains, which we consider arcs when generating the disconnected graphs. We then build a hierarchical graph representation from the distributed disconnected graphs connecting the graphs of adjacent subdomains. This approach minimizes inter-node communications in the

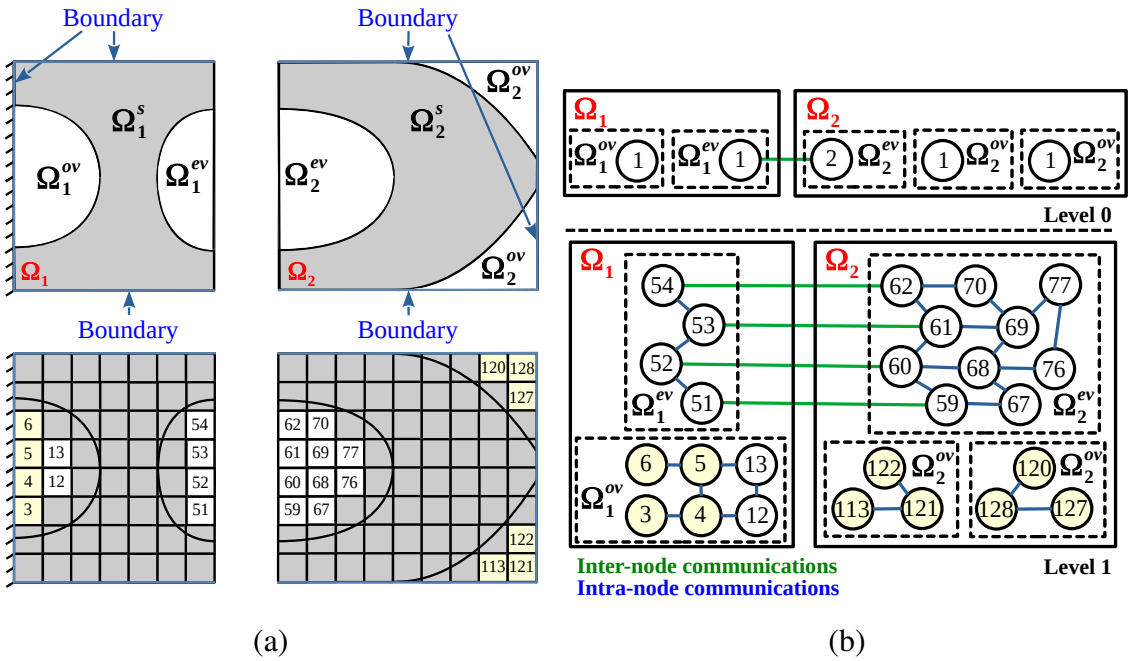

Figure 2: Detection of distributed enclosed holes: (a) the multiply connected structure and the binarized design field labeled by boundary edges, and (b) the hierarchical undirected distributed graph for detecting holes and classifying them into opened and enclosed ones (green arcs indicate inter-node communications).

classification of the domain Ω^v. We have to remark that classifying the distributed disconnected graphs requires a recursive process to verify that the classification is coherent. This recursive process requires inter-node communications, but using the hierarchical representation ensures reduced bandwidth use.

Figure 2(a) shows the design domain Ω divided into two subdomains $\Omega = \Omega_1 \cup \Omega_2$ containing the corresponding solid and void domains per subdomain. We tessellate both subdomains and label the elements containing some edge or face in the boundary. Figure 2(b) shows the undirected graphs generated by each subdomain from the tessellated domain considering the elements of the domain $\Omega^v = \Omega_1^v \cup \Omega_2^v$. We use the same approach as the serial counterpart to classify the disconnected graphs. It also shows the hierarchical representation adopted for inter-node communications. One can observe in this simple example that the inter-node communications decrease meaningfully using Level 0 of the hierarchical representation instead of Level 1.

3 Topology optimization framework

We adopt the density-based topology optimization approach to find the optimal material distribution with prescribed mechanical properties from scratch, i.e., without

making any assumptions about the design configuration. Assuming the material interpolation model of equation (1) with a penalization power $p \geq 3$ to ensure that we do not violate the Hashin-Shtrikman bounds, we relax the minimum compliance topology optimization problem to allow using gradient-based optimization approaches.

3.1 Classical formulation

We can formulate the minimum compliance topology optimization as minimizing the structural compliance as follows

$$\begin{aligned} \min_{\boldsymbol{\rho}} \quad & c(\tilde{\boldsymbol{\rho}}) = \mathbf{f}^{\mathrm{T}}\mathbf{u}(\tilde{\boldsymbol{\rho}}) \\ \text{s. t. :} \quad & \mathbf{K}(\tilde{\boldsymbol{\rho}})\mathbf{u}(\tilde{\boldsymbol{\rho}}) = \mathbf{f} \\ : \quad & E(\tilde{\boldsymbol{\rho}}) = E_{min} + \tilde{\rho}^p \left(E_0 - E_{min}\right) \\ : \quad & V(\boldsymbol{\rho}) - V^* \leq 0,\ \rho(x) \in [0,1], \end{aligned} \tag{3}$$

where $\tilde{\boldsymbol{\rho}}$ is the regularized design field, $\mathbf{K}(\tilde{\boldsymbol{\rho}})$ is the global stiffness matrix, $\mathbf{u}(\tilde{\boldsymbol{\rho}})$ and $\mathbf{f}$ are the global displacement and force vectors, $E(\tilde{\rho})$ is the artificial elastic modulus with $E_{min} > 0$ for empty material, and $V(\boldsymbol{\rho})$ is the volume fraction of the design limited by the target volume V^*.

We can impose a length scale constraint by filtering the design field $\boldsymbol{\rho}$ to obtain a well-posed topology optimization problem, proving Bourding [18] the existence of solutions in this setting. We perform the convolution product of the design field $\boldsymbol{\rho}$ with the filter F as $\tilde{\rho}(x) = (F * \rho)(x)$ with $\int_{B_R} F(x) = 1$, being B_R an open ball of radius $R > 0$ with $F \geq 1\ \forall x \in B_R$. In practice, we use the following expression

$$\tilde{\rho}(x) = \frac{\sum_{e \in N_e} w(\mathbf{x}_e) v_e \rho_e}{\sum_{e \in N_e} w(\mathbf{x}_e) v_e}, \tag{4}$$

where $\tilde{\boldsymbol{\rho}}$ represents the filtered design field, v_e is the elemental volume, N_e is the neighborhood set of elements lying within the radius R, and $w(\cdot)$ is a conic weighting function $w(\mathbf{x_e}) = R - ||\mathbf{x_e} - x||_2$.

We can define the implicit form of the convolution integral for the density filter on the domain $\Omega \subset \mathbb{R}^n$ as the solution of the following Helmholtz differential equation with homogeneous Neumann boundary conditions

$$\begin{aligned} -r^2\nabla^2\hat{g} + \hat{g} = g \qquad & \hat{g} \in \Omega \\ \frac{\partial \hat{g}}{\partial \mathbf{n}} = 0 \qquad & \hat{g} \in \partial\Omega \end{aligned} \tag{5}$$

where g is the nodal vector of design variables, $\hat{g}$ is the filtered field, and r is a length parameter playing a similar role as the radius R of the convolution integral for calculating the density filter. We can obtain a relationship between length scales to configure the equivalent r parameter to the corresponding physical radius R of the convolution integral. We approximate the projections between nodal and elemental g variables using interpolation functions. We can solve this problem efficiently using a parallel solver. After obtaining the nodal values of the filtered field $\hat{g}$, the filtered sensitivity for a given element is obtained by averaging the nodal values of the filtered field [19].

To use gradient-based optimization methods, we calculate the sensitivity of (3) to the design variable ρ using the chain rule as follows

$$\frac{\partial c(\tilde{\rho})}{\partial \rho} = \frac{\partial c(\tilde{\rho})}{\partial \tilde{\rho}} \frac{\partial \tilde{\rho}}{\partial \rho}, \tag{6}$$

where $\mathbf{u}^*$ is given by the solution of the adjoint problem $\mathbf{K}\mathbf{u}^* = \dfrac{\partial c(\tilde{\boldsymbol{\rho}})}{\partial \mathbf{u}} = \mathbf{f}$, whose solution is $\mathbf{u}^* = \mathbf{u}$ because the minimization of the structural compliance is self-adjoint, obtaining the different terms as

$$\frac{\partial c(\tilde{\rho})}{\partial \tilde{\rho}} = -\mathbf{u}^*(\tilde{\boldsymbol{\rho}})^{\mathrm{T}} \frac{\partial \mathbf{K}(\tilde{\boldsymbol{\rho}})}{\partial \rho} \mathbf{u}(\tilde{\boldsymbol{\rho}}) \tag{7}$$

$$\frac{\partial \tilde{\rho}}{\partial \rho} = \frac{w(\mathbf{x}_i) v_i}{\sum_{i \in N_e} w(\mathbf{x}_i) v_i} \tag{8}$$

3.2 Manufacturing constraints

We can introduce a penalization scheme of the enclosed cavities detected during the topology optimization process. To do so, we define the φ variable as follows

$$\varphi(\rho(x), \Omega^{ev}) = \begin{cases} 1 - \rho(x), & \text{if } x \in \Omega^{ev} \\ 0, & \text{otherwise} \end{cases}, \tag{9}$$

reintroducing the φ variable in the design one using a maximum function $\xi = max(\rho, \varphi)$, smoothing it using the p-norm as follow

$$\tilde{\xi} = (\rho^q + \varphi^q)^{1/q}. \tag{10}$$

We can then formulate the structural minimization problem as follows:

$$
\begin{aligned}
\min_{\boldsymbol{\rho}} \quad & c(\tilde{\boldsymbol{\xi}}) = \mathbf{f}^{\mathrm{T}}\mathbf{u}(\tilde{\boldsymbol{\xi}}) \\
\text{s. t. :} \quad & \mathbf{K}(\tilde{\boldsymbol{\xi}})\mathbf{u}(\tilde{\boldsymbol{\xi}}) = \mathbf{f} \\
: \quad & E = E_{min} + \tilde{\xi}^p \left(E_0 - E_{min}\right) \\
: \quad & V(\boldsymbol{\rho}) - V^* \leq 0,\ \rho(x) \in [0,1], \\
: \quad & g_{ev} \leq g_{ev}^*
\end{aligned}
\tag{11}
$$

where $\tilde{\xi} \approx max(\bar{\tilde{\rho}}, \varphi)$ is the smoothed maximum of regularized and projected design field $\bar{\tilde{\rho}}$ and the φ field penalizing the enclosed voids, $\mathbf{K}(\tilde{\boldsymbol{\xi}})$ is the global stiffness matrix, $\mathbf{u}(\tilde{\boldsymbol{\xi}})$ and $\mathbf{f}$ are the global displacement and force vectors, $E(\tilde{\xi})$ is the artificial elastic modulus with $E_{min} > 0$ for empty material, $V(\tilde{\boldsymbol{\xi}})$ is the volume fraction of the design limited by the target volume V^*, and g_{ev} is the number of disconnected graphs in the domain Ω^{ev} during the topology optimization limited by the target number of empty cavities g_{ev}^*.

We can then calculate the sensitivity of equation (11) to the design variable ρ using the chain rule as follows

$$
\frac{\partial c(\tilde{\xi})}{\partial \rho} = \frac{\partial c(\tilde{\xi})}{\partial \tilde{\xi}} \frac{\partial \tilde{\xi}}{\partial \tilde{\rho}} \frac{\partial \tilde{\rho}}{\partial \rho},
\tag{12}
$$

obtaining the different terms as

$$
\begin{aligned}
\frac{\partial c(\tilde{\xi})}{\partial \tilde{\xi}} &= -\mathbf{u}(\tilde{\xi})^{\mathrm{T}} \frac{\partial \mathbf{K}(\tilde{\xi})}{\partial \rho} \mathbf{u}(\tilde{\xi}) && (13) \\
\frac{\partial \tilde{\xi}}{\partial \tilde{\rho}} &= (\tilde{\rho}^{q-1} - \varphi^{q-1}) \cdot (\tilde{\rho}^q + \varphi^q)^{\frac{1}{q}-1} && (14) \\
\frac{\partial \tilde{\rho}}{\partial \rho} &= \frac{w(\mathbf{x}_i) v_i}{\sum_{i \in N_e} w(\mathbf{x}_i) v_i}, && (15)
\end{aligned}
$$

adopting a continuation strategy by increasing the radius R to ensure the convergence of the optimization until we satisfy the constraint $g_{ev} - g_{ev}^* \leq 0$ of the optimization problem (11).

3.3 Parallel framework

We organize the stages of density-based topology optimization using a modular parallel architecture. The modules group the calculations required by some functionality. The framework consists of several modules providing the required functionalities by

the topology optimization approach. The underlying idea is to facilitate the configuration of different modules, reusing code already tested using other algorithms or topology optimization techniques. We also can configure these modules for serial or parallel computing, requiring a different compiler and compatibility with diverse libraries. We describe the organization of modules and functionalities below.

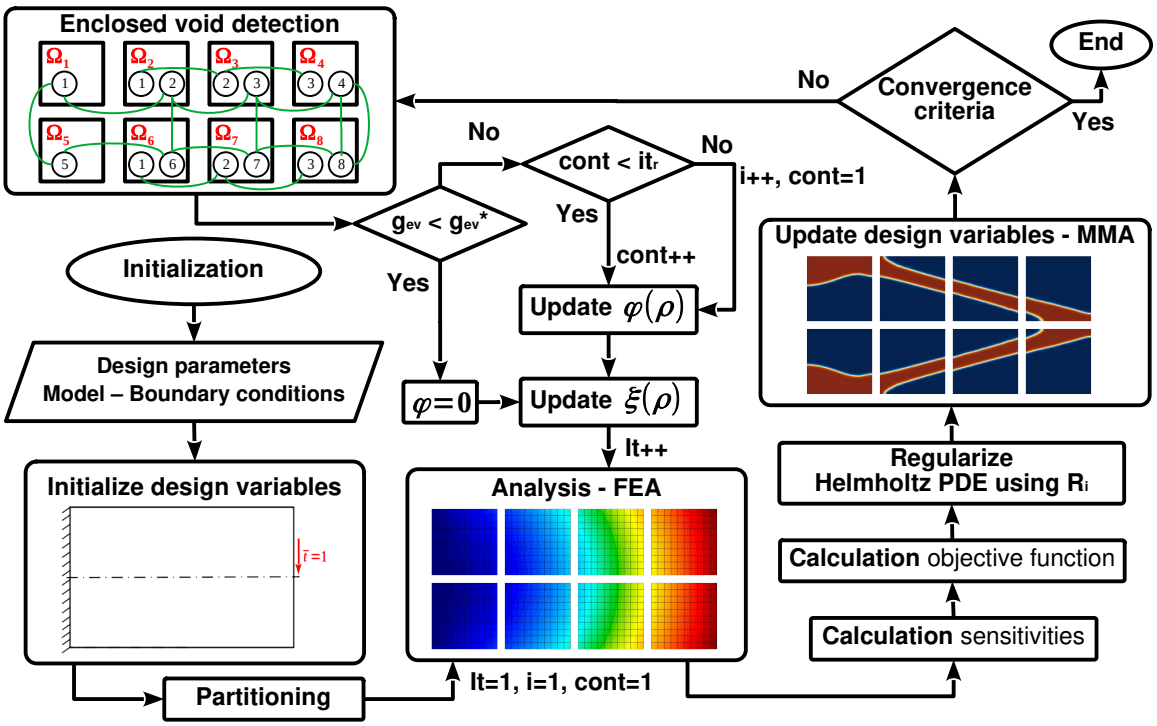

Figure 3: Flowchart of density-based topology optimization incorporating manufacturing constraints using parallel computing.

The initialization module defines the design parameters and boundary conditions of the model. It also initializes the design field that satisfies the volume constraint of density-based topology optimization approaches. The partitioning module divides the domain into many subdomains following some criteria, such as minimizing the interface between subdomains. This module generates a dual graph from the mesh, where each element becomes a vertex, and the common nodes of elements become arcs between elements. The method then uses a multilevel k-way partitioning approach [20] to obtain the subdomains. The analysis module implements the solver adopted for solving the system of equations from the PDE governing the physics of the problem. We can select serial and parallel computing, usually using the former for the initial development and debugging and the latter for addressing large-scale models. It supports direct and iterative solvers, preconditioning the latter using Algebraic Multigrid (AMG) and Geometric Multigrid (GMG) methods.

The regularization module implements the filter for density-based topology opti-

mization formulation. In this case, we use the Helmholtz PDE with homogeneous Neumann boundary conditions filter, which is more efficient for parallel computing using different regularization distances R. The module to update the design implements the Method of Moving Asymptotes (MMA) using parallel computing. The sensitivity and objective function calculations are straightforward because they only use elemental information. Finally, the enclosed void detection module implements the technique presented in Section 2.

Figure 3 shows the flowchart of the parallel implementation of the distributed density-based topology optimization incorporating manufacturing constraints using the modules presented above. One can observe that the partitioning module divides the problem into many subdomains to perform the recursive stages of the density-based topology optimization method. In particular, the analysis module uses FEA to solve the system response, and the corresponding modules calculate the objective function and sensitivities, regularize the design field, and update the design variables. The proposed method to detect the enclosed cavities operates on the corresponding subdomains.

4 Numerical experiments

This section shows the preliminary results of the modified formulation presented in Section 3.2 for incorporating manufacturing constraints in minimum compliance topology optimization. The formulation requires the identification and classification of void cavities. We compare the designs using the classical and modified formulations using a simple two-dimensional cantilever problem to show the ability of the method to remove enclosed void cavities. The two-dimensional cantilever problems consist of locating a punctual load at the center of the end cantilever using asymmetric simplications. We set the target volume V^* to 25% of the volume of the initial domain. We impose the initial length scale constraint with a radius R of size doubling the element size, incrementing its value in the same initial magnitude every 30 iterations for the continuation strategy until we satisfy the constraint $g_{ev} - g_{ev}^* \leq 0$.

We evaluate the cumulative timing for both the classical topology optimization formulation and the modified one introducing manufacturing constraints. The cumulative timing aims to show the computing benefits of the proposal scaling with the computing resources. We use up to three computers connected through a 10 Gbps Ethernet for running the experiments. These computing nodes incorporate two E5-2687W v4 CPUs and 256 GB of RAM. The CPUs include 12 cores working at 3.0 GHz, running up to 24 processes in parallel per computing node.

Figure 4(a) shows the geometric configuration and boundary conditions of the cantilever problem with one punctual load at the cantilever's endpoint. We can observe the definition of boundaries at all the edges of the cantilever. Figure 4(b) shows the antisymmetric simplification for the structural analysis, the mesh, and an example with

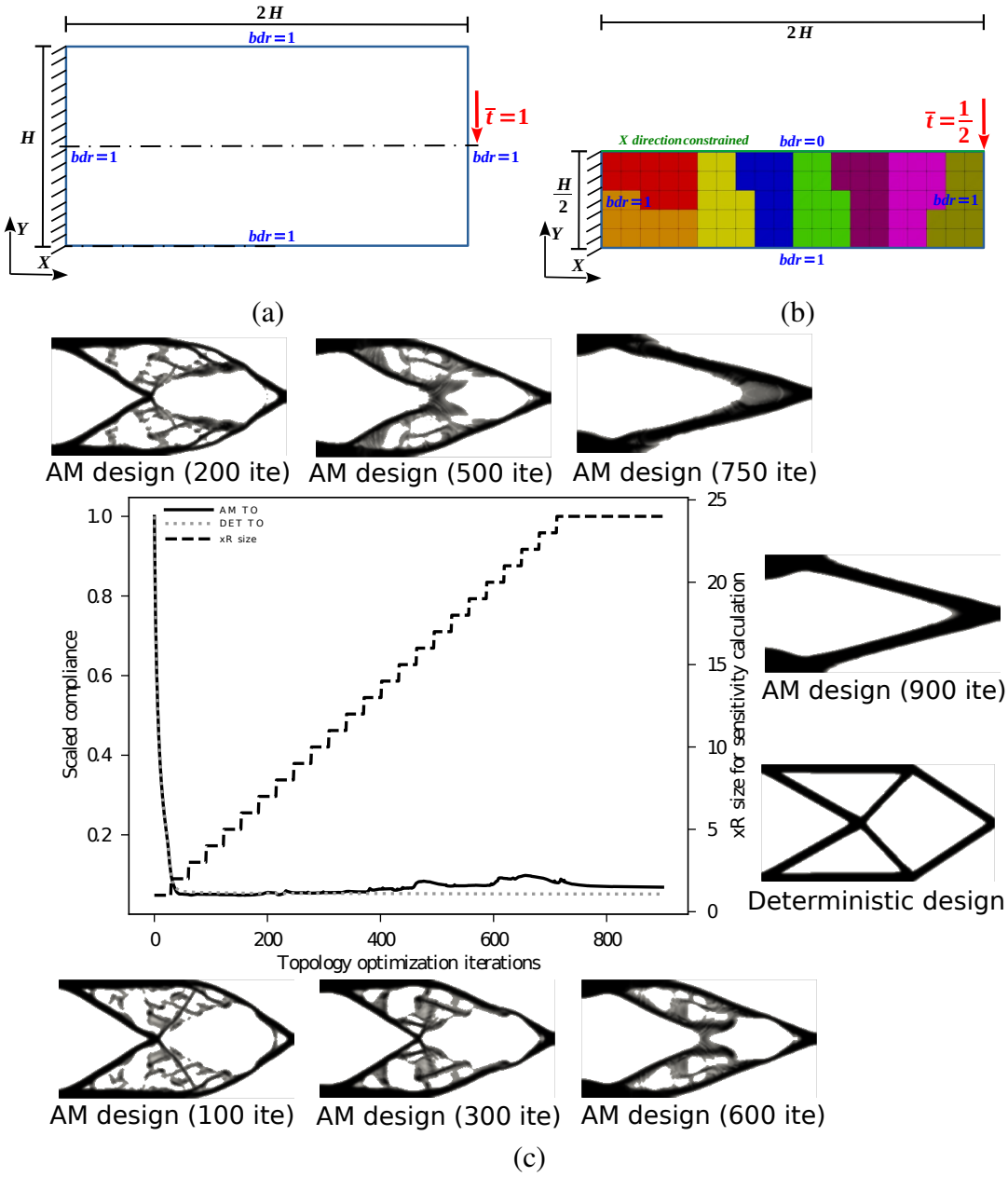

Figure 4: Cantilever experiment: (a) Geometric configuration and boundary conditions, (b) tessellated domain divided into eight subdomains with asymmetric simplifications, and (c) evolution of the objective function of deterministic and manufacturing-constrained topology optimizations.

eight subdomains used for parallel computing the topology optimization problem. We can observe that we do not constrain the symmetry axis as a boundary in the empty hole detection method introduced in Section 3.2. Figure 4(c) shows the evolution of compliance during the topology optimization process. One can observe how the regularization radius R increases until we remove the enclosed void cavities satisfying

the constraint $g_{ev} \leq 0$. The design introducing manufacturing constraints has not enclosed voids, whereas the deterministic design shows three enclosed holes.

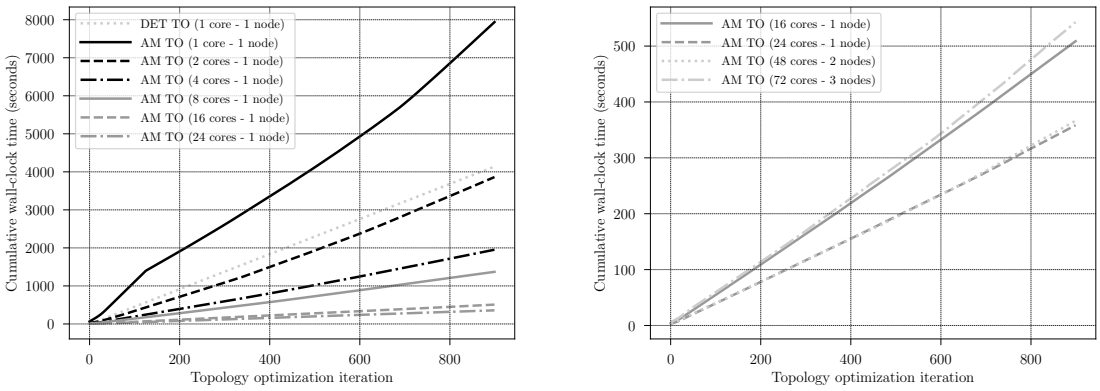

(a) (b)

Figure 5: Strong scaling of cantilever experiment 2 using a grid of 320×160 (51200) linear elements (103362 DoFs): cumulative wall-clock time using (a) a different number of cores in the same core and (b) using a different number of computing nodes.

Figure 5 shows the strong scaling experiment for evaluating the scalability of the approach with computing resources. It shows the cumulative wall-clock time for the topology optimization using different numbers of subdomains to assess the use of several cores in one computing node and using up to three computing nodes. We can observe that the performance increases with the number of cores in the same computing node. However, the improvements decrease by introducing more computing nodes. We can attribute this fact to inter-node communications, which are much slower than intra-node communications. Inter-node communications also can generate bandwidth problems.

5 Concluding remarks

We aim to introduce manufacturing constraints in topology optimization to avoid empty material cavities in the final designs, which generate problems in many additive manufacturing processes. Incorporating these constraints in the design allows to manufacture the high-performance designs directly using ALM techniques. We present a novel approach to detecting enclosed void cavities from the design variable information. We implement this technique using parallel computing with distributed memory. We also incorporate the method to detect the enclosed holes into a minimum compliance topology optimization formulation as manufacturing constraints.

The numerical experiments show that the proposal is feasible for obtaining designs

without empty material cavities. The experiments compare the design performance using the minimum compliance formulation and incorporating the manufacturing constraints. One can observe that the minimized compliance slightly increases by introducing the manufacturing constraints w.r.t. the classical topology optimization formulation. The numerical experiments also show that the proposal can be incorporated into a distributed topology optimization framework, achieving speedups of up to 14x using 24 cores w.r.t. the serial implementation of the topology optimization approach. All these developments will allow us to address real-world problems incorporating manufacturing constraints in future works.

Acknowledgements

We acknowledge the support of the AEI/FEDER and UE under contract no. DPI2016-77538-R and Airbus Operations S.L. under contract no. ONIERE 7528/23ECEG and CHALUPA 7756/23ECEG.

References

[1] J. Liu et al., "Current and future trends in topology optimization for additive manufacturing", Struct. Multidisc. Optim., 57, 2457–2483, 2018.

[2] M.P. Bendsøe and O. Sigmund, Topology Optimization – Theory, Methods, and Applications, second edition, Springer-Verlag Berlin Heidelberg, 2004.

[3] J. Pou, A. Riveiro, and J.P. Davim, Additive Manufacturing (Handbooks in Advanced Manufacturing), first edition, Elsevier, 2021.

[4] S. Liu, Q. Li, W. Chen, L. Tong, and G. Cheng, "An identification method for enclosed voids restriction in manufacturability design for additive manufacturing structures", Front. Mech. Eng., 10(2), 126–137, 2015.

[5] Q. Li, W. Chen, S. Liu, and L. Tong, "An identification method for enclosed voids restriction in manufacturability design for additive manufacturing structures", Struct. Multidisc. Optim., 54:971–984, 2016.

[6] C. Wang, B. Xu, Q. Meng, J. Rong, and Y. Zhao, "Numerical performance of Poisson method for restricting enclosed voids in topology optimization", Comput. Struct., 239, 106337, 2020.

[7] A. Donoso, E. Aranda, and D. Ruiz, "A new approach based on spectral graph theory to avoiding enclosed holes in topology optimization", Comput. Methods Appl. Mech. Engrg., 393, 114769, 2022.

[8] Y. Xiong, S. Yao, Z-L. Zhao, and Y.M. Xie, "A new approach to eliminating enclosed voids in topology optimization for additive manufacturing", Additive Manufacturing, 32, 101006, 2020.

[9] Y. He, Z-L. Zhao, X. Lin, and Y.M. Xie, "A hole-filling based approach to controlling structural complexity in topology optimization", Comput. Methods Appl. Mech. Engrg., 416, 116391, 2023.

[10] Q. Wang, H. Han, C. Wang, and Z. Liu, “Topological control for 2D minimum compliance topology optimization using SIMP method”, Struct. Multidisc. Optim., 65(38), 2022.
[11] D. Herrero-Pérez and S.G. Picó-Vicente, “A parallel geometric multigrid method for adaptive topology optimization”, Struct. Multidisc. Optim., 66(225), 2023.
[12] D. Herrero-Pérez and P. Martínez-Castejón, “Multi-GPU acceleration of large-scale density-based topology optimization”, Adv. Eng. Softw., 157–158(103), 103006, 2021.
[13] D. Herrero-Pérez, S.G. Picó-Vicente, and H. Martínez-Barberá, “Adaptive density-based robust topology optimization under uncertain loads using parallel computing”, Eng. Comput., 40, 21–43, 2024.
[14] D. Herrero-Pérez and S.G. Picó-Vicente, “Adaptive fail-safe topology optimization using a hierarchical parallelization scheme”, Comput. Struct., 291, 107205, 2024.
[15] M. Bendsøe and O. Sigmund, “Material interpolation schemes in topology optimization”, Arch. Appl. Mech., 669(9–10), 635–654, 1999.
[16] S.B. Myers, “Connections between Differential Geometry and Topology”, Proceedings of the National Academy of Sciences of the United States of America, 21(4), 225–227, 1935.
[17] R.E. Korf, “Depth-first iterative-deepening: An optimal admissible tree search”, Artif. Intell., 27(1), 97–109, 1985.
[18] B. Bourdin, “Filters in topology optimization”, Int. J. Numer. Methods Eng., 50(9), 2143–2158, 2001.
[19] B.S. Lazarov and O. Sigmund, “Filters in topology optimization based on Helmholtz-type differential equations”, Int. J. Numer. Methods Engng., 86(6), 765–781, 2011.
[20] G. Karypis and V. Kumar, “Multilevel k-way partitioning scheme for irregular graphs”, J. Parallel Dist. Com., 48(1), 96–129, 1998.